

Author responses to comments of Reviewer n. 1 for the manuscript “Assessing the spatial and temporal variability of methylmercury biogeochemistry and bioaccumulation in the Mediterranean Sea with a coupled 3D model”

The paper describe a modelling study of Hg cycle in the Mediterranean Sea using a high resolution regional model. It is a very interesting and important modelling effort since It is the first attempt to simulate this contaminant in this region with a coupled dynamical-biogeochemical model. The paper is well written and results are globally well illustrated and discussed. The modelling approach considers the main Hg species in the ocean and the related processes that control their exchanges and redistributions. The analysis focuses on MeHg species that represent the toxic species for ecosystems, and investigates the transfer and bioaccumulation in the low trophic level, the planktonic reservoir (phytoplankton and zooplankton). It provides very new interesting and quantified informations on the spatial and temporal distribution of MeHg species in the different regions of the Mediterranean Sea. I then recommend this paper for publication, but suggest also some major revision on the description of the model. The paper focuses mainly on MeHg species, but the cycling of Hg in the Mediterranean sea is controlled by the distribution and exchange among all the different species that are not well document in this paper, while it is of importance to assess the consistency of the results.

Recently an assessment of Mercury in the Mediterranean Sea has been published (Cossa et al, 2022). It provides constraints on sources of hg in the Mediterranean Sea (atmospheric, riverine, sediments), exchange fluxes at Gibraltar with the Atlantic Ocean, and budget of THg and MeHg in the western and Eastern basin. I suggest that before publication, this paper compares in its supplementary material, its modelling results with the budget derived by this Mediterranean Hg assessments, in order to verify that the global modelling approach is coherent with observations.

Cossa et al. *Mediterranean Mercury Assessment 2022: An Updated Budget, Health Consequences, and Research Perspectives*. *Environ. Sci. Technol.* 2022, 56, 3840–3862

We will follow the reviewer’s advice and, in addition to the comparison with observed concentrations MeHg (Fig. 5) and total Hg (Fig. S11) we propose to introduce a wider discussion on important terms of the budget of Hg species as follows:

- We propose to reorganize the manuscript to include an additional sensitivity simulation that we have recently run which consider higher Hg loading and POC inputs from rivers, to explore the model uncertainty regarding the fate of river loads of particulate Hg. We will add a new subsection “Sensitivity simulation for river Hg load” to the Methods, and a new subsection on “Model sensitivity and uncertainty” to the Results. The text for the new subsections is provided at the end of this document.
- We will compare modelled net atmospheric exchange of Hg⁰ and total inorganic Hg with other estimates (Cossa et al., 2022; Gencarelli et al., 2014; Zagar et al., 2007) as reported in the text of the subsection “Model sensitivity and uncertainty” provided below.
- We will add a comparison of modelled yearly outflow of Hg and MeHg to the Atlantic Ocean with the estimate from the budget of Cossa et al., (2022), as reported in the text of the subsection “Model sensitivity and uncertainty” provided below.

We believe that further analysis and details on the complete budget of Hg species deserve to be assessed in a future work running ad-hoc simulations including routines for high-frequency calculation of fluxes. We indeed aim at developing such a work supported by additional field observations (of Hg concentrations and fluxes) and sensitivity analyses (e.g., on model initial conditions and/or biogeochemical parameterizations) to achieve a best quantification of fluxes and uncertainties, also exploring intra- and interannual variability of Hg dynamics.

2.3.3 Sensitivity simulation for river Hg load

The largest Mediterranean rivers are characterized by proximal-accumulation-dominated dispersal system, i.e., deltaic systems with fast and substantial (>50-90%) sediment accumulation in the proximity of their mouth (Walsh and Nittrouer, 2003). Consistently with this picture, a recent budget for the Mediterranean Sea estimated that the magnitude of total Hg input from rivers (6 Mg y⁻¹) is comparable to the Hg flux to the shelf sediments (6.8 Mg y⁻¹), suggesting that most of the Hg associated with riverine particles settle before reaching the open ocean (Cossa et al., 2022). We, therefore, included only the dissolved load of Hg and MMHg in the reference simulation and explored the uncertainty related to this choice with a sensitivity simulation accounting for the total load Hg species, i.e., including both the particulate and dissolved inputs of HgII and MMHg. Limited data are available to characterize the spatial and temporal variability of these sources. The most robust observations are from a time-series (2008-2010) for the Rhône River (Cossa et al., 2017) indicating 0.85 ± 0.45 nmol g⁻¹ of HgT and 0.017 ± 0.008 nmol g⁻¹ of MMHg. Assessments in the Ebro River, impacted by an industrially polluted water reservoir, and in the Po River, which drain the largest Italian industrial and agricultural areas, found respectively 4.9 nmol g⁻¹ and 1.15 nmol g⁻¹ of particulate HgT at the river mouth, also highlighting the role of episodic stormy event in transporting large amounts of particles and associated pollutants (Palanques et al., 2020, Vignati et al., 2003). Further, at the mouth of the Soča/Isonzo River, impacted by upstream Hg mining, concentrations of unfiltered Hg higher than 200 pM have been reported (Hines et al., 2000). Hg loads for the Mediterranean tributary were estimated based on this information as synthesized in Tab. S6, also qualitatively referring to the spatial distribution of Hg stock and erosion fluxes in European topsoils (Panagos et al., 2021) and other information on anthropogenic activities (Ahmed et al., 2018). In the reference simulation, including only the dissolved input, the loading estimate is 0.28 Mg y⁻¹ for total dissolved Hg (and 0.008 Mg y⁻¹ for dissolved MMHg), while in the simulation with total Hg inputs the loading is about 4.6 Mg y⁻¹ including 0.27 Mg y⁻¹ of MMHg. Despite the relatively high mean concentrations (Tab. S6) assumed, the estimated HgT load is slightly lower than the estimate (6 Mg y⁻¹) from Cossa et al., (2022), most likely because the water discharge used in that work (>350 km³ y⁻¹) is higher than the total discharge used in this model setup (>291 km³ y⁻¹). On the other hand, the load to the Mediterranean Sea from solely European rivers (2.9 Mg y⁻¹) estimated from Hg concentrations in topsoils and water erosion rates from river catchments (Panagos et al., 2021) is slightly lower than the load from European rivers in our model setup (3.25 Mg y⁻¹). Finally, all these estimates are lower than the 18 Mg y⁻¹ computed by (Liu et al., 2021) for the Mediterranean Sea through a global river model explicitly considering water discharge, suspended solids, and Hg loadings. Based on these calculations, Liu et al., (2021) proposed a global river load (1000 Mg y⁻¹) much higher than the estimate from the latest global mercury assessment (300 Mg y⁻¹) (UNEP, 2018). They also estimated that the 70% of the load is buried in coastal and shelf sediment.

3.1 Model sensitivity and uncertainty

The sensitivity analysis showed that the sinking rate of organic detritus (POC) is an important control on the vertical distribution of MeHg (i.e., the shape of the vertical profile) along the water column but has little effect on the values of MeHg concentrations maxima, and on the distribution of inorganic Hg species (Supplemental Sect. S1.1 and Figs. S1 and S2). On the other hand, the increase of sinking velocity from 3 to 10 m d⁻¹ improved the agreement of modelled seasonal fluxes of POC at 200 m depth with available observations (Ramondenc et al., 2016) (Supplemental Sect. S1.1 and Fig. S3). The sensitivity also showed that the increase in the coefficient for Hg methylation (x_{met}) results in a best agreement with observed MeHg concentrations (Cossa et al., 2022, 2009), while the inclusion of DOC remineralization flux results in an overestimation of surficial MeHg concentrations (Supplemental Sect. S1.2 and Fig. S3).

The inclusion of higher riverine HgII, MMHg, and POC inputs does not improve the agreement between modelled and observed concentrations of MeHg (Supplemental Sect. S1.3 and Figs. S5-S10), suggesting that the underestimation of MeHg maxima in subsurface waters is not due to an underestimation of watershed sources. These results also corroborate the idea that a substantial fraction of particulate Hg and MeHg carried by rivers settles in coastal areas along with POC (Fig. S5), as estimated in a recent budget based on field observations (Cossa et al, 2022). Nonetheless, large uncertainties in the spatial

and temporal variability of riverine loadings and coastal processes remain to be addressed both at the basin and global scale (Cossarini et al., 2021, Liu et al., 2021).

The underestimation of MeHg in the model does not appear to be related to inorganic Hg availability, since the concentrations of HgT are within the experimental uncertainty of the data (Fig. S11).

Modelled fluxes of HgT and Hg0 compare well with other budget estimates (Cossa et al., 2022, Žagar et al., 2007). The net exchange of Hg0 with the atmosphere indicates 44.8 Mg y⁻¹, which is close to a previous estimate (50 Mg y⁻¹) based on aquatic biogeochemical modelling (Žagar et al., 2007) and slightly lower than the flux adopted in the budget from Cossa and coauthors (67.5 Mg y⁻¹). The net exchange of Hg species (~7 Mg y⁻¹) is here significantly lower than the estimate (29.8 Mg y⁻¹) from Cossa et al., (2020). However, while the latter estimate is based on an atmospheric model assuming a constant ocean surface Hg0 concentrations (Gencarelli et al., 2014), here, the flux is estimated accounting for 3D dynamics in the marine system, including sequestration of Hg species from surface waters due to the biological carbon pump. Recent evidence from isotopes studies pointed out that the ocean might be a net sink for atmospheric Hg, rather than a net source (Jiskra et al., 2021).

The modelled export of HgT from the Alboran Sea to the Atlantic Ocean is 9.3 Mg y⁻¹, close to the value (9.7 Mg y⁻¹) estimated by Cossa et al., (2022). On the other hand, our estimate (2.5 Mg y⁻¹) of MeHg outflow is significantly lower than the 5.6 Mg y⁻¹ of the budget by Cossa et al., (2022), even assuming an increased value for x_{met} and, consequently of subsurface MeHg.

All in all, a calibration of the parameter x_{met} appears appropriate based on the current understanding, also considering that the initial guess for this parameter come from a global ocean application (Zhang et al., 2020). Indeed, such a global model study underestimated the observed MeHg concentrations in the Mediterranean Sea, while reproducing with good agreement, or overestimating, observations from various cruises in the North Atlantic and Pacific Ocean, pointing out the need to better resolve spatial and temporal variability of biological processes and linked Hg dynamics (Zhang et al., 2020). A comprehensive validation of the OGSTM-BFM biogeochemical variables (Cossarini et al., 2021) highlighted good model accuracy in surface water but higher mismatches with observed oxygen and nutrients concentrations in the mesopelagic zone, attributed to uncertainties in remineralization and deep ventilation processes, which also affect methylation dynamics. In spite of uncertainties remaining to be addressed, the OGSTM-BFM-Hg model is able to reproduce the spatial gradients observed in the Mediterranean Sea, testifying the improvements in capability to simulate Hg dynamics (Žagar et al., 2014, 2007) through the coupling with key biological processes, e.g. the carbon pump and microbial loop (Bowman et al., 2020; Cossa et al., 2017, 2009; Heimbürger et al., 2010; Monperrus et al., 2007; Munson et al., 2018; Sunderland et al., 2009).

Supplemental Material

Supplemental Section S1.3. Sensitivity to Hg river loadings

The sensitivity analysis on Hg input from rivers was performed by implementing two simulations aimed at being representative of the lower (0.28 Mg y⁻¹) and upper bound (4.6 Mg y⁻¹) of river loadings (Sect. 2.3.3 in the main text). The load of organic particles from rivers, previously not included in the model setup, was added to account for the effects of coastal sedimentation, assuming an average concentration of 5 mg l⁻¹ for all the rivers (Burgeois et al., 2011). This attempt to include coastal dynamics is still a first approximation for several reasons including the limited spatial and temporal coverage of data to validate coastal processes (Cossarini et al., 2021; Liu et al., 2021) and the absence in this model of a tracer for inorganic solids load.

The comparison between the modeled POC fluxes at 200 m depth and the observational dataset compiled by Ramondenc et al., (2016) performed to validate the test on sinking velocity (Supplemental Sect. 1.1) was

repeated for the simulation including riverine POC sources against the reference simulation, showing very limited to no changes in the fluxes in the open waters (Fig. S5).

The results showed little sensitivity of the Hg state variables in the open waters to the prescribed variation in river loadings, as the impacts are mostly limited to coastal areas in the vicinity of major rivers (Fig. S6). The highest impacts are in surface waters (0-500 m depth) (Figs. S7-S9) and variations minimum at greater depths (e.g., Fig. S10). In the western subbasins, the variation of Hg species and Hg_T concentrations in surface waters (Figure S7) is mostly in the range 1-2%, except for an increase of 3-7% in the most surficial layers (0-100 m) of the *Nwm* influenced by the high discharge of the Rhône River. In the eastern subbasins, there is more variability in response (Figs. S8-S10): the highest increases are in the coastal subbasin *Nad* (about 20% for Hg_T and >25% for MMHg) that receive high Hg loadings from the Po and Soca/Isonzo Rivers, also affecting the southernmost confining subbasin *Sad* (with variation of 10-20% for Hg_T and about 10% for MMHg in the upper 100 m). The easternmost and shallowest part of the Levantine Sea (*Lev4*) also shows relatively high variations (4-7% for Hg_T and MMHg in the first 100 m), while the impacts are lower (1-4%) in the other subbasins. Overall, these results imply small variation in modelled concentrations, and it should be noted that excluding the shallow *Nad* subbasins, the variations in MMHg concentrations are maxima at the top of the water column where concentrations are very low (<0.02-0.06 pM).

Figure S3. Seasonal dynamics of Particulate Organic Carbon fluxes in various subbasins of the Mediterranean Sea. The fluxes calculated from monthly mean model output are shown for the two simulations (Supplemental Sect. S1.1) assuming $w_s = 3 \text{ m d}^{-1}$ (dashed blue line for the average and shaded area for minimum and maximum values) and $w_s = 10 \text{ m d}^{-1}$ (solid black line and grey shaded area), compared with observations (red dots and bars indicate the seasonal median and the I and III quartiles) compiled by Ramondenc et al., (2016).

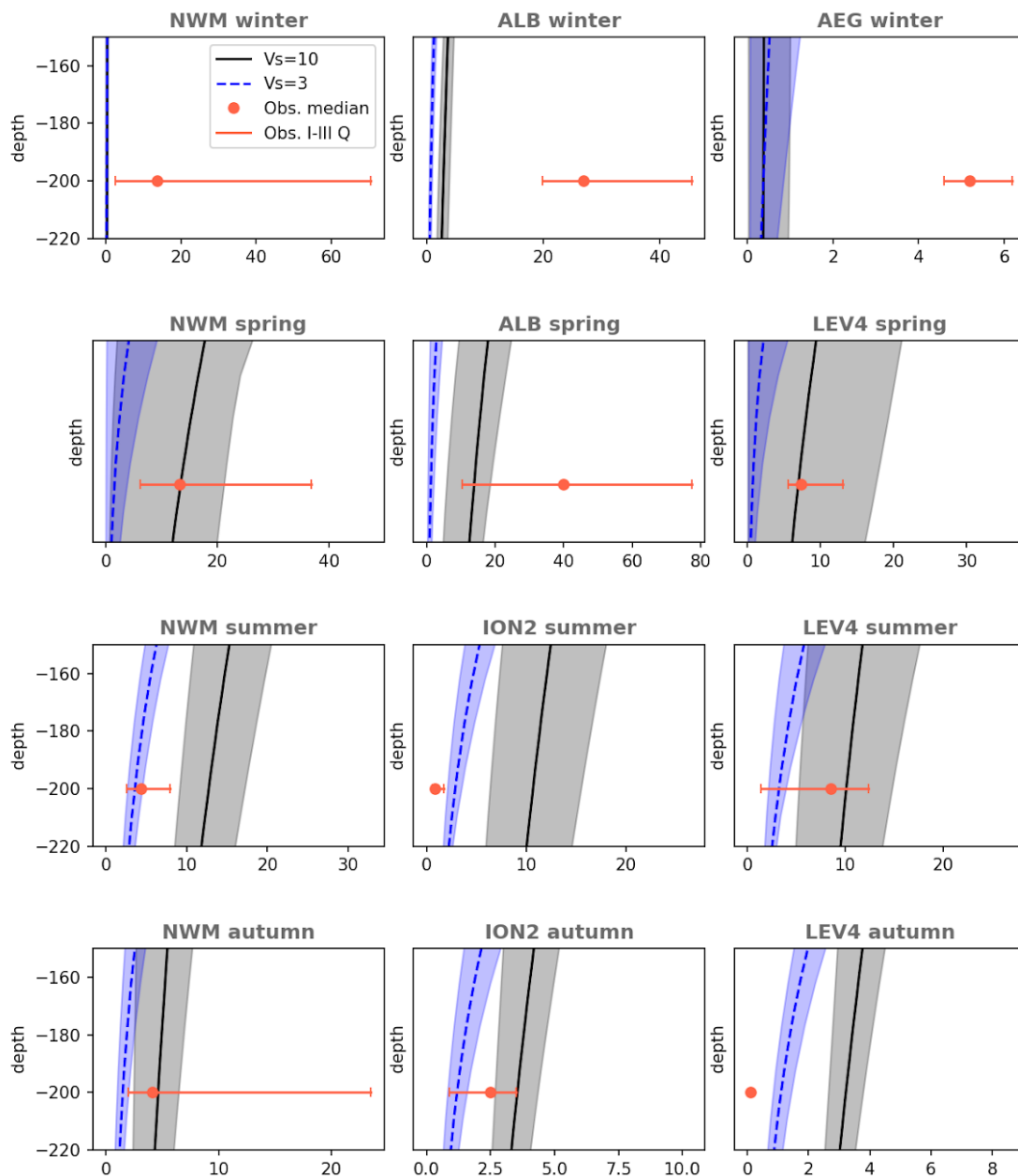


Figure S5. Seasonal dynamics of Particulate Organic Carbon fluxes in various subbasins of the Mediterranean Sea. The fluxes calculated from monthly mean model output are shown for the simulation with POC input from rivers (dashed blue line for the average and shaded area for minimum and maximum values) and for the reference simulation including only dissolved river inputs (solid black line and grey shaded area) (Supplemental Sect. S1.3), compared with observations (red dots and bars indicate the seasonal median and the I and III quartiles) compiled by Ramondenc et al., (2016).

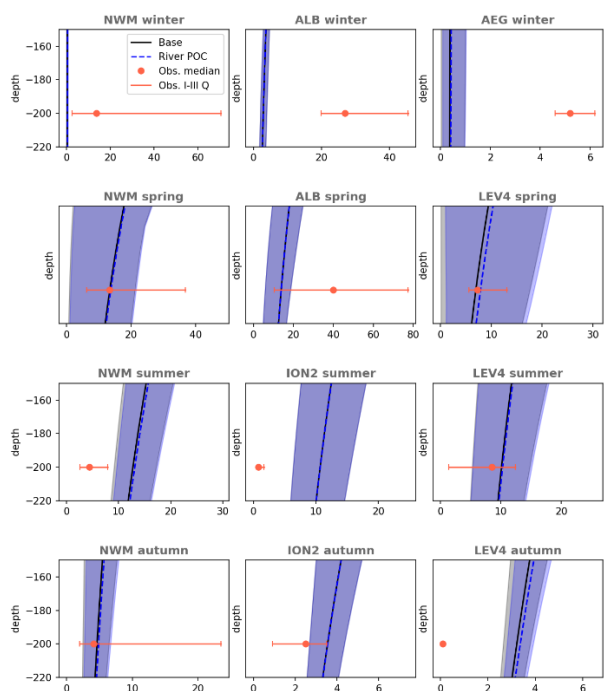


Figure S6. Spatial distribution of the variation (%) in modelled concentration of Hg^{II} for the simulation including input of particulate Hg from river (Supplemental Sect. S1.3) at different depths (25 m, 60 m, and 100 m) and months (January, April, July, and October).

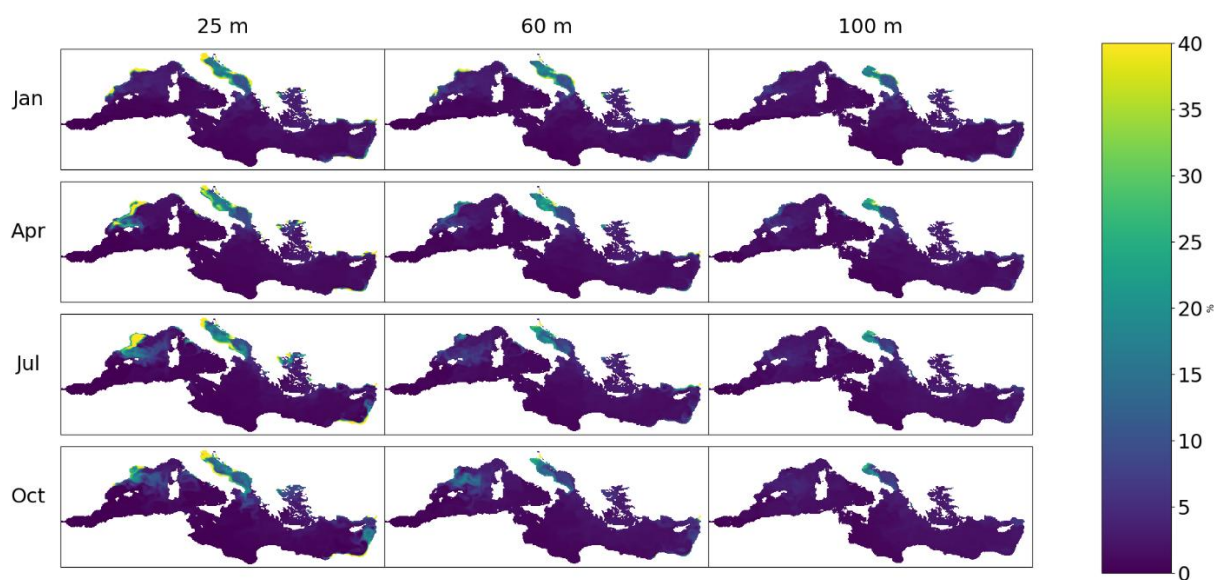


Figure S7. Impact of the simulation with high riverine Hg loads (Supplemental Sect. S1.3) on the seasonal average concentration profiles in surface waters (0-500 m depth) of different subbasins of the Western Mediterranean Sea (*Alb*, *Nwm*, *Swm*, and *Tyr*). The % variation with respect to the reference simulation is shown for each Hg species (Hg^{II} : yellow dashed line, Hg^0 : dotted cyan line, MMHg: dash-dotted purple line, DMHg: dotted violet line).

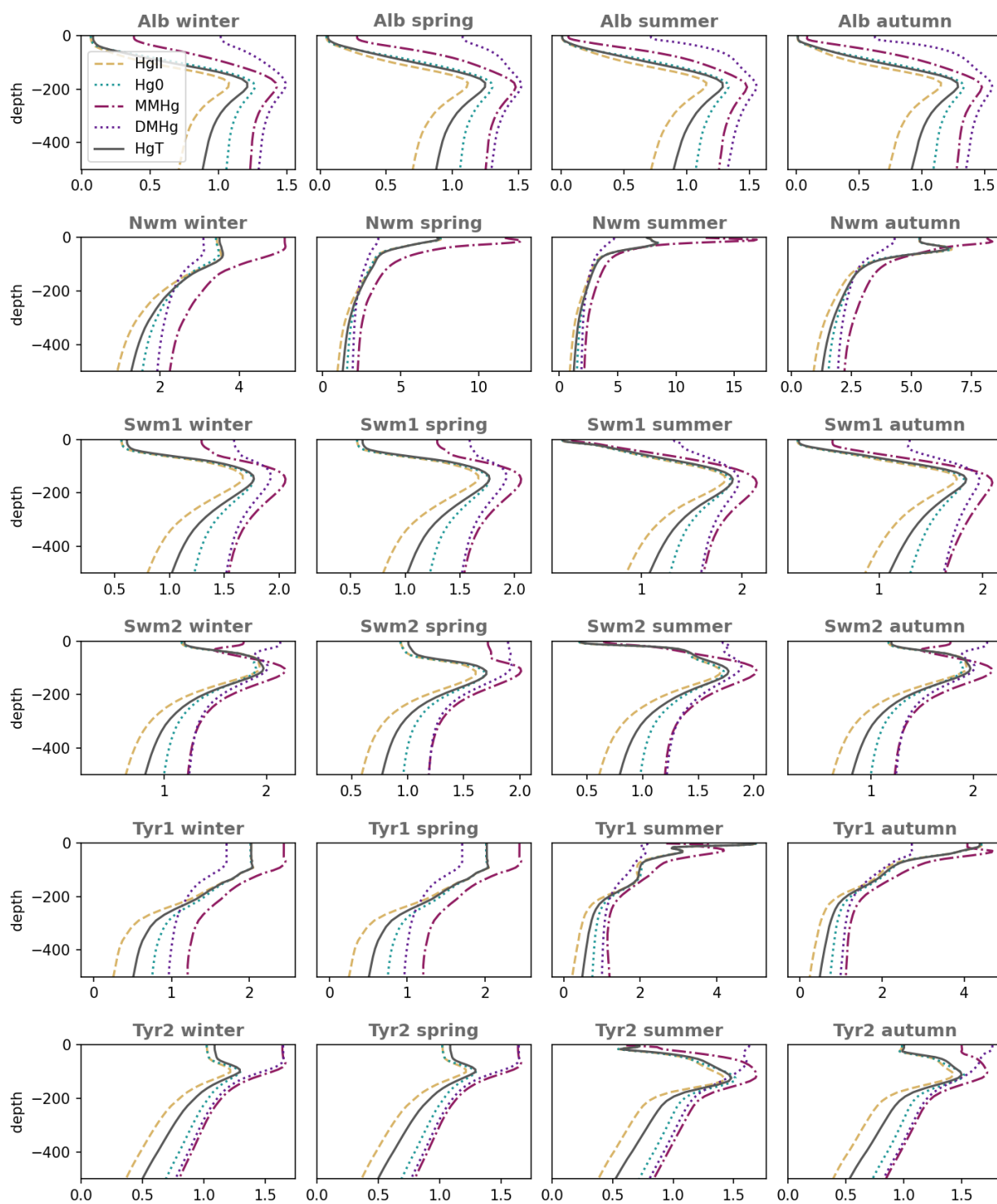


Figure S8. Impact of the simulation with high riverine Hg loads (Supplemental Sect. S1.3) on the seasonal average concentration profiles in surface waters (0-500 m depth) of different subbasins of the Eastern Mediterranean Sea (*Nad*, *Sad*, *Aeg*, and *Lev*). The % variation with respect to the reference simulation is shown for each Hg species (Hg^{II} : yellow dashed line, Hg^0 : dotted cyan line, MMHg: dash-dotted purple line, DMHg: dotted violet line).

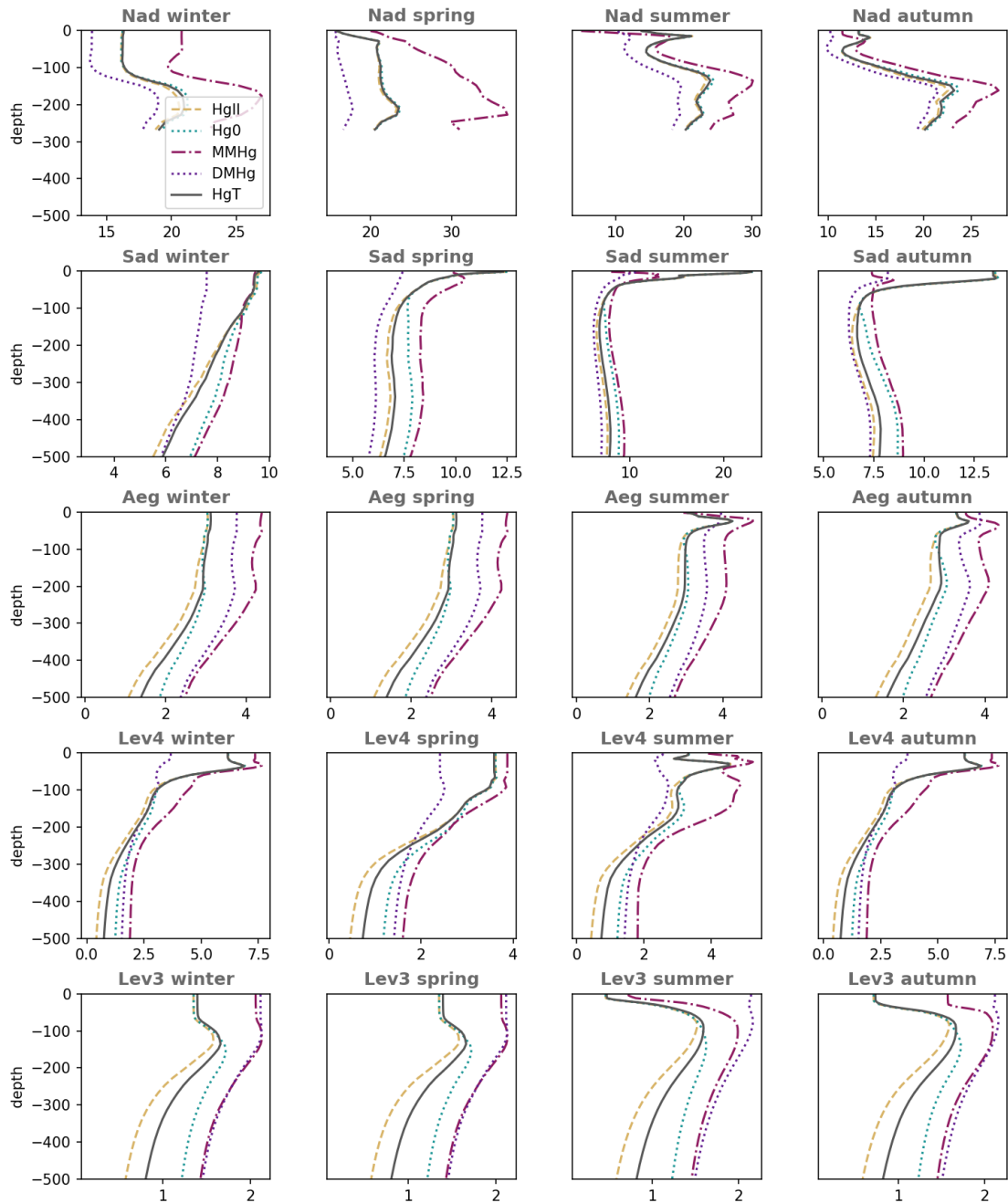


Figure S9. Impact of the simulation with high riverine Hg loads (Supplemental Sect. S1.3) on the seasonal average concentration profiles in surface waters (0-500 m depth) of different subbasins of the Eastern Mediterranean Sea (*Ion and Lev*). The % variation with respect to the reference simulation is shown for each Hg species (Hg^{II} : yellow dashed line, Hg^0 : dotted cyan line, MMHg: dash-dotted purple line, DMHg: dotted violet line).

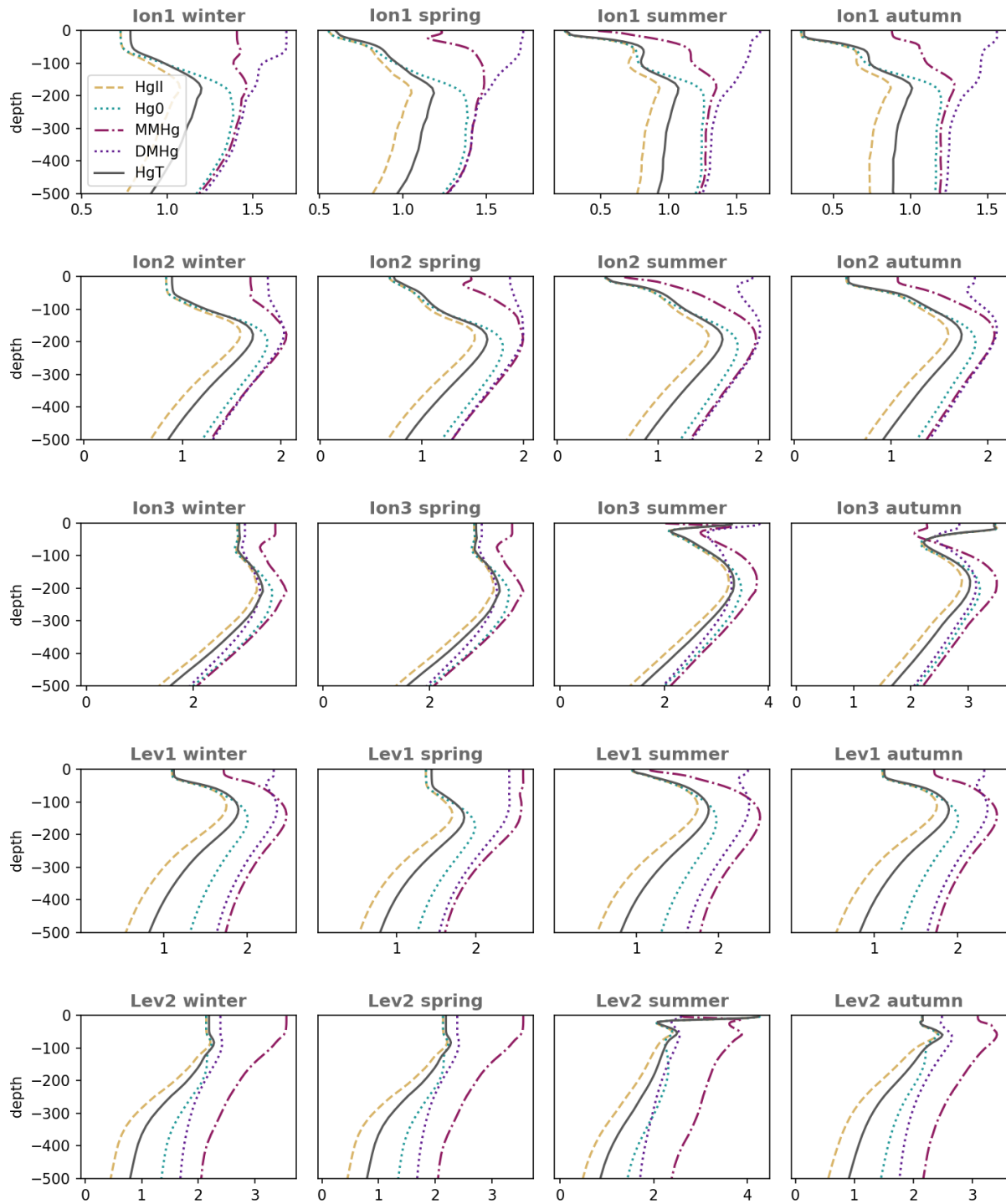


Figure S10. Impact of the simulation with high riverine Hg loads (Supplemental Sect. S1.3) on the seasonal average concentration profiles in the water column of different subbasins of the Eastern Mediterranean Sea (*Ion and Lev*). The % variation with respect to the reference simulation is shown for each Hg species (Hg^{II} : yellow dashed line, Hg^0 : dotted cyan line, MMHg: dash-dotted purple line, DMHg: dotted violet line).

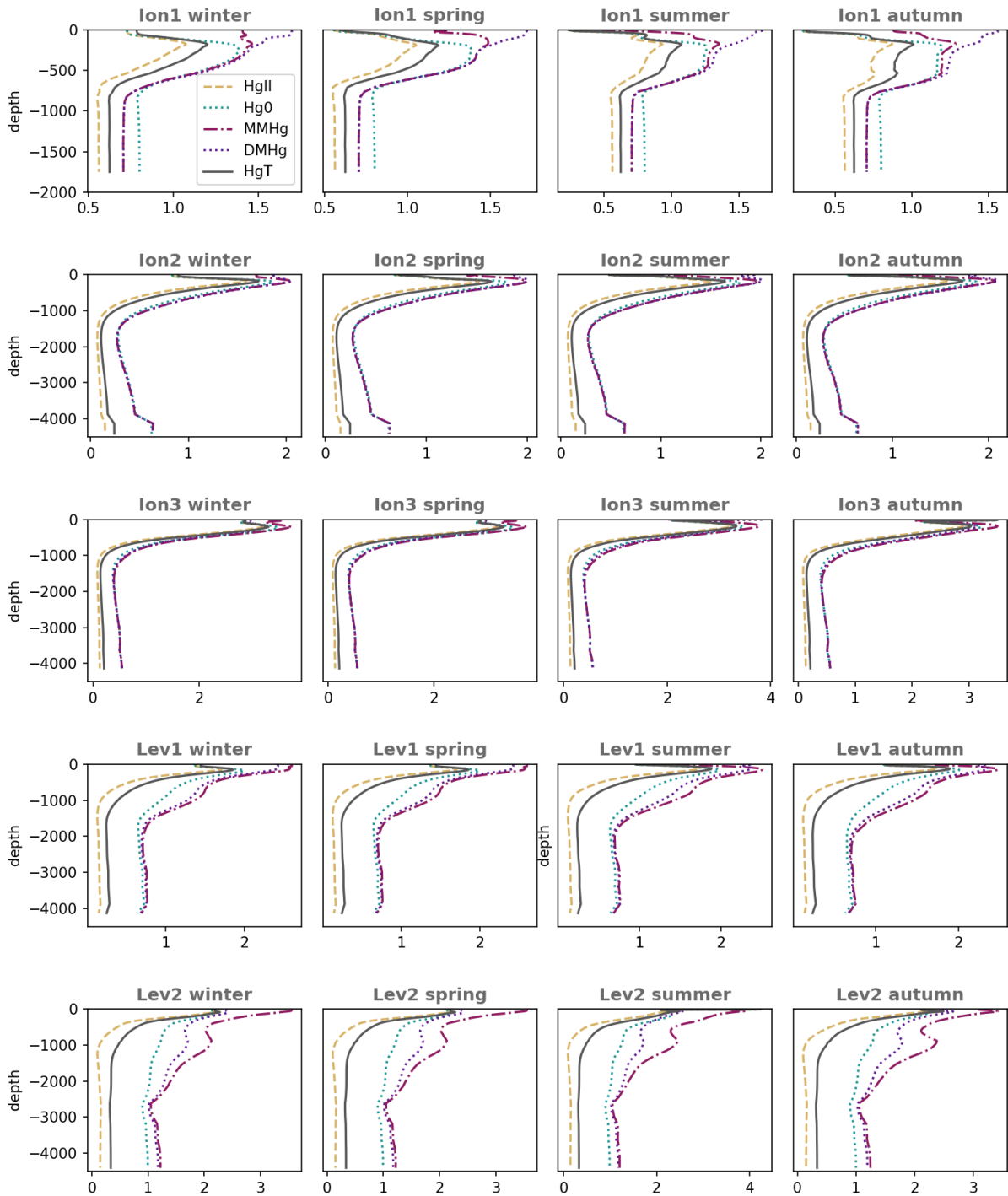


Table S6. Concentrations of riverine HgT and MMHg used in the model setup, and resulting annual load

River Name	HgT	MMHg	HgT	MMHg	Notes and References
	pM	pM	Mg y ⁻¹	Mg y ⁻¹	
Grand Rhone	53	1.06	0.62	0.0355	<i>HgP = 0.85 nmol/g</i> ⁽¹⁾
Petit Rhone	53	1.06	0.07	0.0039	<i>SPM = 60 mg/l</i> ⁽²⁾
Soca/sonzo	170	1.02	0.23	0.0294	<i>90-249 pM at the river mouth</i> ⁽³⁾
Ebro	102	2.04	0.23	0.0070	<i>HgP = 4.98 nmol/g</i> ⁽⁴⁾ <i>SPM = 20 mg/l</i> ⁽⁴⁾
Po Maistra	120	2.4	0.06	0.0030	<i>HgP = 1.15 nmol/g</i> ⁽⁵⁾ <i>SPM = 30 mg/l</i> ⁽⁵⁾
Po Tramontana	120	2.4	0.14	0.0071	
Po Dritta	120	2.4	0.39	0.0201	
Po Scirocco + Po Bonifazi	120	2.4	0.12	0.0062	
Po Bastimento	120	2.4	0.05	0.0028	
Po Bocca Tolle	120	2.4	0.20	0.0102	
Po Gnocca	120	2.4	0.21	0.0106	
Po Goro	120	2.4	0.13	0.0067	
Po Levante	120	2.4	0.02	0.0010	
Po Volano	120	2.4	0.01	0.0003	
Nile	120	2.4	0.28	0.0074	<i>Impacted by Artisanal Small-Scale Gold Mining</i> ⁽⁶⁾
Nile	120	2.4	0.28	0.0074	
Tevere/Tiber	100	2	0.07	0.0136	<i>High mineral Hg content in soils</i> ⁽⁷⁾
Tevere/Tiber	100	2	0.07	0.0136	
Reno	80	1.6	0.03	0.0012	<i>Impacted by Industries and Agriculture</i> ⁽⁷⁾
Vjiose	53	1.06	0.04	0.0026	
Seman	53	1.06	0.02	0.0012	
Buna/Bojana	53	1.06	0.10	0.0060	
Buna/Bojana	53	1.06	0.10	0.0060	
Piave	53	1.06	0.05	0.0030	
Tagliamento	53	1.06	0.03	0.0018	
Livenza	53	1.06	0.04	0.0023	
Brenta-Bacchiglione	53	1.06	0.07	0.0038	
Adige	53	1.06	0.08	0.0049	
Lika	53	1.06	0.02	0.0014	
Krka	53	1.06	0.02	0.0010	
Arno	53	1.06	0.03	0.0017	
Neretva	53	1.06	0.07	0.0043	
Aude	53	1.06	0.03	0.0015	
Trebisjnica	53	1.06	0.03	0.0017	
Mati	53	1.06	0.03	0.0018	

Volturno	53	1.06	0.02	0.0009
Shkumbini	53	1.06	0.02	0.0010
Struma/Strymonas	53	1.06	0.02	0.0014
Merik/Evros/Maritsa	53	1.06	0.05	0.0028
Axios/Vardar	53	1.06	0.03	0.0016
Arachtos	53	1.06	0.02	0.0014
Pinios	53	1.06	0.02	0.0011
Acheloos	53	1.06	0.03	0.0019
Gediz	53	1.06	0.02	0.0012
Buyuk Menderes	53	1.06	0.04	0.0024
Kopru	53	1.06	0.04	0.0022
Manavagat	53	1.06	0.06	0.0032
Seyhan	53	1.06	0.07	0.0038
Ceyhan	53	1.06	0.07	0.0042
Goksu	53	1.06	0.09	0.0051
Medjerda	53	1.06	0.03	0.0017
Asi/Orontes	53	1.06	0.03	0.0015
Total Load (Mg y⁻¹)			4.62	0.27

(1) Cossa et al., 2017; (2) Bourgeois et al., 2011; (3) Hines et al., 2000; (4) Palanques et al., 2020; (5) Vignati et al., 2003; (6) Ahmed et al., 2018; (7) Panagos et al., 2021